AIAA JOURNAL
Vol. 45, No. 4, April 2007

Characteristics of the Tip Leakage Vortex in a Low-Speed Axial Compressor

Yu Xianjun,* Liu Baojie,† and Jiang Haokang†
Beijing University of Aeronautics and Astronautics, 100083 Beijing, People's Republic of China

DOI: 10.2514/1.25530

The flowfields in the tip region of the rotor passage are investigated from a large-scale low-speed axial compressor test at both the design and near-stall conditions by using stereoscopic particle image velocimetry. The characteristics of the tip leakage vortex (TLV) are analyzed based on the variations of its trajectory, concentration, size, streamwise velocity, and the blockage effect, which are extracted from both the ensemble- and conditional-averaged results. According to the ensemble-averaged performance of the TLV, its evolution procedures can be divided into several distinct flow phases. As the flow phase of the TLV changes, its mean flow characteristics also change accordingly. The TLV is inherently unsteady and features unsteady behaviors of vortex wandering, splitting, and breakdown, which have profound effects to its mean flow characteristics.

Nomenclature

A	=	compressor axial direction
A_b	=	local reduced throughflow area caused by the TLV
A_e	=	area of the TLV
A_p	=	local throughflow area of the blade passage
B_A	=	area-based blockage coefficient
B_m	=	mass-flow-based blockage coefficient
C	=	length of the rotor tip chord
D	=	diameter of the TLV
H	=	blade span length
L	=	distance downstream of the blade leading edge
m_b	=	local reduced mass flow rate caused by the TLV
m_t	=	total mass flow rate of the compressor
N_B	=	the number of instantaneous snapshots with reverse flow in the TLV at a measurement plane
N_T	=	the total number of instantaneous snapshots at a measurement plane
PW	=	blade passage width normal to the blade tip chord
R	=	compressor radial direction
Re_{chord}	=	blade chord-based Reynolds number
T	=	compressor tangential direction
U	=	velocity component in the X direction
V	=	velocity component in the Y direction
V_{tip}	=	blade tip speed
W	=	velocity component in the Z direction
W_{mean}	=	the mean value of W in the TLV
W_{min}	=	the minimum value of W in the TLV
X	=	in-plane coordinate of measurement planes, approximately to the compressor radial direction
Y	=	in-plane coordinate of measurement planes, nearly normal to the blade tip chord
Z	=	out-of-plane coordinate of measurement planes, approximately to the flow streamwise direction
ρ	=	air density
Ω	=	rotor rotational speed
ω_{peak}	=	conditional-averaged peak vorticity in the TLV
ω_z	=	out-of-plane component vorticity

Subscripts

C	=	center of the TLV
ext	=	outer edge of the core of the TLV

I. Introduction

TIP leakage flows are of great engineering importance when designing modern axial fans and compressors because of their large impact on pressure rise, efficiency, and stability [1–3]. Investigation of the tip leakage flow in turbomachinery has been a topic of interest for more than half a century. Numerous and extensive experimental studies have been conducted to investigate the tip leakage flow/vortex in both cascades and compressors to determine its flow mechanisms and evaluate the aerodynamic losses it causes [4–13]. Based on these abundant experimental results, the evolution mechanisms of the tip leakage flow/vortex and its influences on the performance of compressors are clarified further. However, it is still the most confusing phenomenon in compressors, because most of the previous experimental results were obtained just in cascades or at the exits of the rotor passage. Hence, the detailed flow states of the tip leakage flow/vortex inside the rotor passage should be well investigated for further analyses.

It is well known that the tip leakage vortex (TLV) is inherently highly unsteady. However, traditional measurement techniques, such as hot wire, laser Doppler velocimetry, and aeroprobe, can hardly capture its unsteady flow structures. These measurement tools are all point-based techniques, and the data they obtain should be processed by methods involving some types of statistical description, such as ensemble averaging. To overcome this difficulty, the particle image velocimetry (PIV) technique, an instantaneous planar velocimetry technique, was employed for turbomachinery investigation nearly 20 years ago. It has been a routine technique and is widely used in turbomachinery at present. Some researchers investigated the tip leakage flow/vortex in compressor tests by using stereoscopic PIV (SPIV) [14,15]. In contrast, the measurement planes in their works just spanned the blade-to-blade surfaces, which makes the analyses of the detailed kinematic and dynamic properties of the TLV difficult, because the TLV is a streamwise vortex, and the information in its cross planes is much more useful. Recently, Liu and coworkers used SPIV in an axial compressor by placing the two CCD cameras at different sides of the laser light sheet, making the measurement plane possibly span the hub-to-tip surfaces, and obtaining detailed unsteady flow information of the TLV inside the

Received 31 May 2006; revision received 6 November 2006; accepted for publication 28 November 2006.

*Ph.D. Student, School of Jet Propulsion, Group 404, National Key Laboratory on Aeroengines.

†Professor, School of Jet Propulsion, Group 404, National Key Laboratory on Aeroengines.

Table 1 Characteristic design parameters of the compressor test facility

Parameter	Value
Outer diameter (m)	1.0
Hub-to-tip ratio	0.6
Design Speed (rpm)	1200
Design mass flow rate (kg/s)	22.4
Flow coefficient	0.58
Pressure rise coefficient	0.48
Re_{chord}	7.5×10^5
IGV-rotor space (mm)	41.9
Configuration	IGV + rotor + stator
Number of blades	36 + 17 + 20
Blade camber angle (degree)	17.4 + 26.5 + 49.1
Blade stagger angle (degree)	10.4 + 33.4 + 12.3
Blade height (mm)	200 + 199 + 198
Blade chord (mm)	100 + 180 + 180
Rotor tip clearance (mm)	1.0
Rotor-stator space (mm)	48.7

rotor passage. According to their experimental data, some new features of the TLV were found [13,16].

In this paper, we will focus on the overall performance of the TLV inside the rotor passage, and analyze the relationship between its ensemble-averaged (steady) and instantaneous (unsteady) behaviors. Hence, both the ensemble-averaged results and the instantaneous snapshots will be considered. According to the experimental results, the growing processes of the TLV can be depicted with different evolution phases at different compressor operating conditions. Moreover, it is found that the ensemble-averaged states of the TLV change with its unsteady behavior between different evolution phases. Based on these analyses, it is hoped that the results of the current study will be helpful in understanding the deep-seated flow mechanisms of the TLV, and in developing flow control methods in the rotor tip region and validating the steady and unsteady CFD codes.

II. Experimental Setup

The measurements reported in this paper were made in the Low-speed Large-scale Axial Compressor Facility (LLACF) of Beijing University of Aeronautics and Astronautics (BUAA). All the data were acquired with SPIV and the phase-locking technique.

A. Compressor Facility

The test facility is a single-stage axial compressor with inlet guide vanes (IGV). A large contraction ratio bellmouth with a 1.8 m outer diameter lemniscate profile equipped with flow straightness is used to provide uniform and steady inlet flow. The rotor and stator blades with C4-series airfoil are designed in terms of the free vortex law. More detailed design parameters are summarized in Table 1. In this study, measurements were conducted at the design point (mass flow coefficient is 0.58) and the near-stall point (mass flow coefficient is 0.39), respectively. For the flow diagnostics of LDV and PIV/SPIV, the casing is fitted with a large curved optical access window, $420 \times 280 \times 5$ mm in length × width × thickness, which is molded to match the contour of the casing wall and locates over the whole compressor stage except for the IGV, as shown in Fig. 1.

B. SPIV Setup and Data Processing

A commercial SPIV system, developed by TSI Incorporation, was employed in the measurement, and a schematic diagram of its installation is shown in Fig. 1. The light source is a dual cavity Nd: YAG laser, and the maximum illumination energy is 150 mJ/pulse at a 15 Hz repetition rate. A pair of 1280×1024 pixels and 12-bit frame-straddling-based CCD cameras (PIVCAM 13-8) were configured in different sides of the laser light sheet in Scheimpflüg condition. In the experiment, two types of fields of view are used as shown in Fig. 2. One is about 200×70 mm, which covers nearly half of the whole blade passage and is used to scan the main flow structures at the investigated region. The other is about 130×50 mm, which is used to detect fine scale structures near the blade tip. The measurements total to 22 cross sections, as shown in Fig. 3, and cover nearly the entire rotor passage; at least 100 instantaneous realizations are recorded at each cross section. TSI Insight 5 and an in-house-developed program are employed for data processing. The images are analyzed with a multipass process, which makes the final velocity vector grid spatial resolutions about

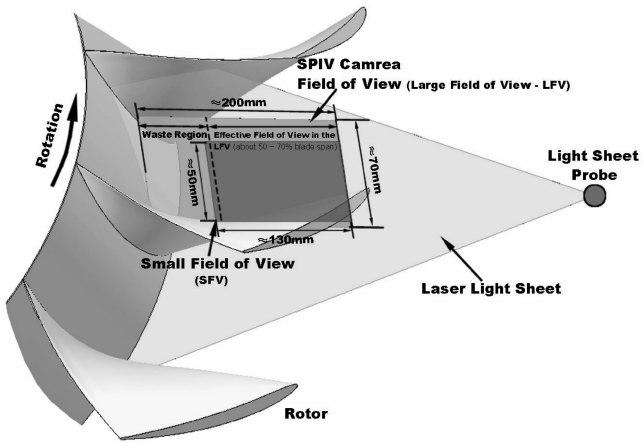

Fig. 2 Schematic of the laser light sheet inside the rotor passage and SPIV camera view field.

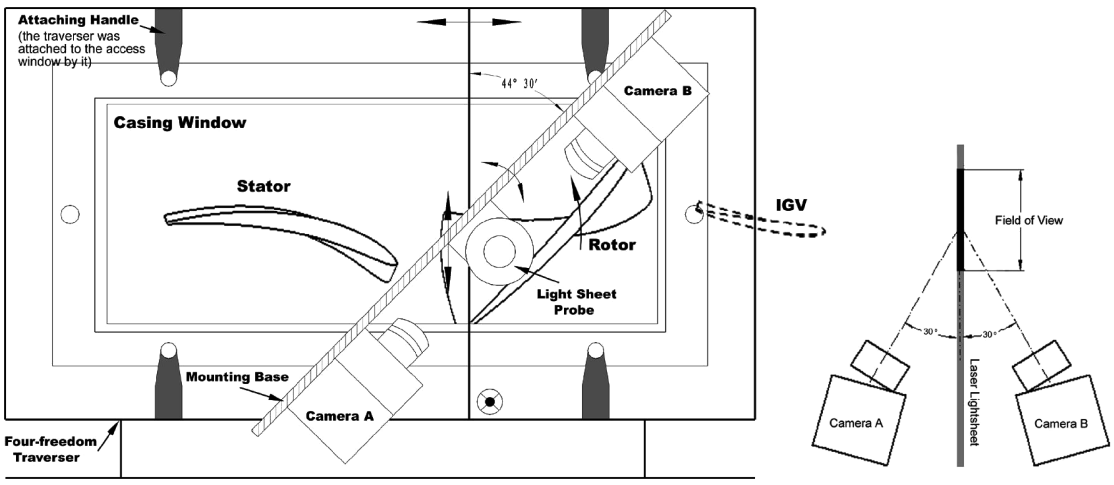

Fig. 1 Schematic of the SPIV installation.

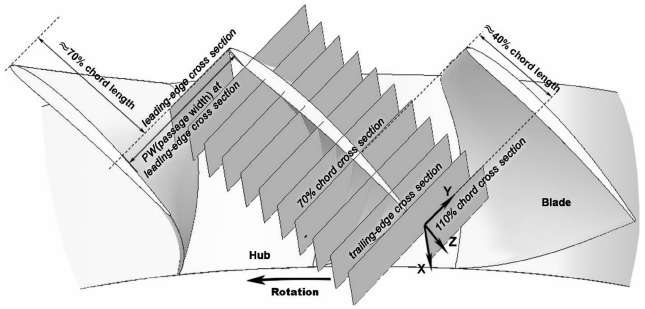

Fig. 3 Schematic layout of SPIV measurement cross sections.

1.15 mm and 0.77 mm for the large field of view (LFV) and small field of view (SFV), respectively. Additional details on the SPIV setup, data acquisition, data processing, and uncertainty estimates have been introduced by Liu et al [16].

C. Experiment Layout

Experiments were conducted at 22 cross sections in the rotor passage at both the design and near-stall conditions. As shown in Fig. 3, near the blade suction surface (SS), the measurement planes perpendicular to the blade tip chord are uniformly arranged from 20% chord downstream of the blade leading edge to 10% chord downstream of the blade trailing edge, with an interval of 10% chord length in the LFV. Additionally, measurements were also conducted at four planes, 10, 20, 30, and 40% chord downstream of the blade leading edge in the SFV. (Because of the geometric restriction of the access window and the rotor blades, the flowfield near the blade leading edge cannot be investigated.) Near the blade pressure surface (PS), all the measurements were conducted in the LFV, and the measurement planes, which are also perpendicular to the blade tip chord, are laid out from the blade leading edge to the blade trailing edge with an interval of 10% chord length. As mentioned, the field of view covers nearly half of a whole blade passage in the LFV. However, the effective field of view covers only 50–70% of the blade span height, which is caused by the combined effects of the geometric restriction of the blade passage and the strong flare light at the hub surface, as shown in Fig. 2. To obtain the data of the whole passage, the measurements along the blade SS and PS were conducted individually with a fixed circumferential position of the CCD cameras by using the phase locking technique; as a result, the corresponding measurement planes of the two groups do not overlap, as can be seen in Fig. 4.

III. Results and Discussion

Based on the analyses made by Liu et al. [16], the uncertainty of the instantaneous velocity in the main flow region is nominally 2.5–4%, and it can achieve 5% below 60% blade span and 7% near the casing wall, for the results in the SFV. It should be noted that the accuracy of the in-plane components are about 2–4%, and it is about 7–14% for the out-of-plane component. As for the instantaneous results obtained in the LFV, their uncertainties are usually 0.5% higher. Averaging 100 instantaneous velocity vector maps together yields ensemble-averaged velocity vector maps with an accuracy of about 2, 6, and 3% in the mainstream region, in the tip region, and in the region below 60% blade span, respectively, whether it is in the LFV or the SFV. Evidently, it was difficult to obtain statistically convergent results in such a complicated experiment with just 100 realizations at each location. To obtain statistically convergent quantities, the data sample size should be larger; possibly, it should be larger than 1000 samples or even more. In a previous study by the

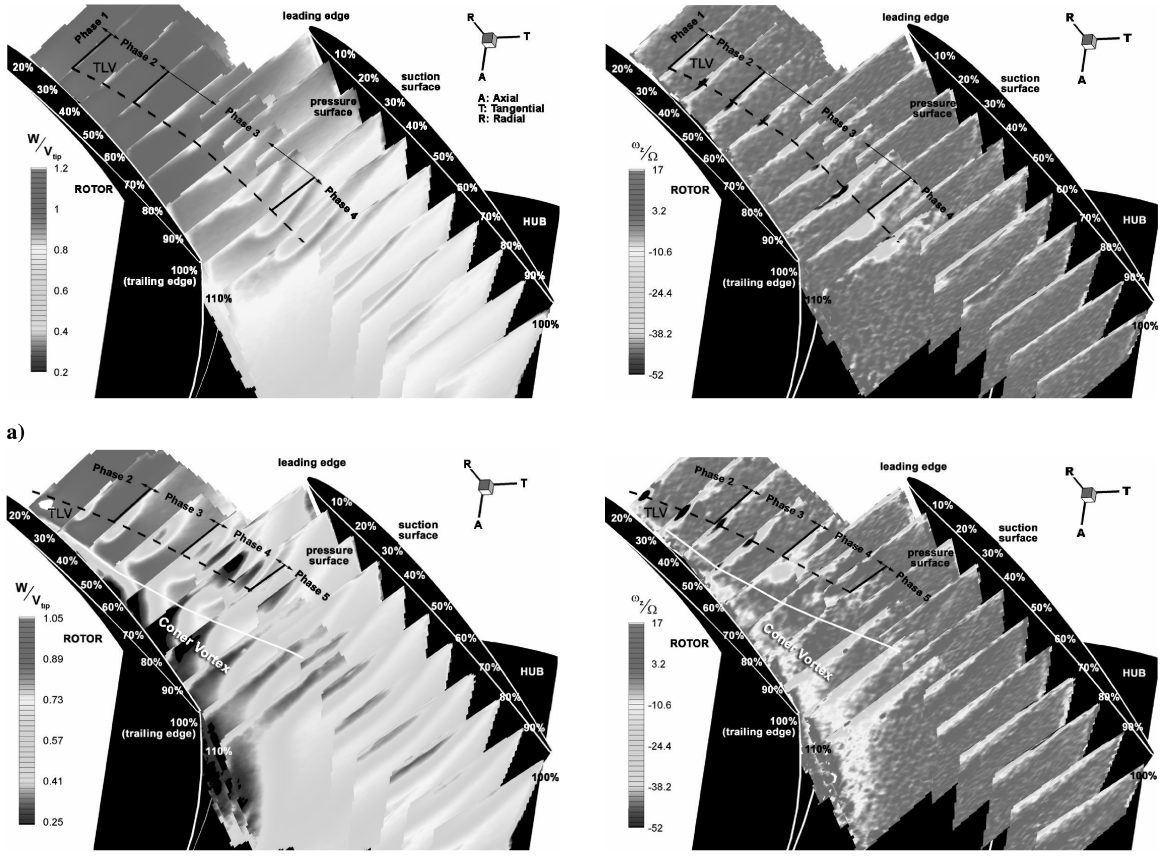

Fig. 4 Combined maps of the ensemble-averaged measured results inside the rotor passage in the relative frame fixed to the rotor at the a) design and b) near-stall conditions. Left: normalized streamwise velocity, W/V_{tip}; right: normalized vorticity, ω_z/Ω. (ω_z is defined positive when a vortex rotates in the same direction as the rotor. The results shown here were all obtained in the LFV.)

current authors [16], the convergence characteristics of the turbulence intensity in some typical measurement planes in a similarly complex flow were determined. It was observed that although there were distinct deviations between the results for 100 and 200 samples in most regions, the trends were consistent even in the region of the tip leakage vortex with vortex breakdown. Thus, although 100 images are inadequate to obtain accurate second-order statistical quantities, such as the vorticity magnitudes shown in the paper, their variation tendencies and orders of their magnitude should be correct.

The flow in compressor rotor features complex 3-D flow structures, such as the tip leakage flow/vortex, the corner vortex, the scraping vortex, and other secondary flows. It can be seen in Fig. 4 that the TLV appears as the most distinct secondary flow structure inside the tested rotor at both the design (DE) and near-stall (NS) conditions.

A. Overall Performance

The trajectories of the TLV can be seen clearly from both the velocity and the vorticity maps in Fig. 4 and are sketched by black dash lines. The TLV appears with high negative vorticity (opposite rotating to the rotor) and low relative streamwise velocity in the vortex core region.

According to the previous work done by Liu et al. [16], at the DE condition, the evolvement of the TLV can be marked off into the following phases:

Phase 1: formation, near $L/C = 0.3$
Phase 2: evolution and expansion, $L/C = 0.3$–0.5
Phase 3: destabilization, $L/C = 0.5$–1.0
Phase 4: turbulence mixing, $L/C > 1.0$

However, at the NS condition, the evolution processes of the TLV are different with that at the DE condition, because the TLV breakdown occurs. The following are the five distinct phases:

Phase 1: formation, near $L/C = 0.1$
Phase 2: evolution and expansion, $L/C = 0.1$–0.4
Phase 3: destabilization, $L/C = 0.4$–0.6
Phase 4: unsteady breakdown, $L/C = 0.6$–0.8
Phase 5: turbulence mixing, $L/C > 0.8$

The features of the different evolution phases of the TLV at both the design and near-stall conditions were stated simply by Liu et al. [13] also. However, their analyses are qualitative and were just based on the changes of the flow structures of the measured velocity and vorticity maps. In the following sections, the quantitative characteristics of the TLV extracted from both the ensemble/conditional-averaged results and the instantaneous snapshots will be analyzed in detail. In addition, the variations of the flow properties in the core of the TLV at its different evolution phases will be shown.

B. Flow Characteristics in Ensemble/Conditional-Averaged Flowfields

To analyze the characteristics of the TLV, some flow parameters such as the location of the vortex center, the peak vorticity in the vortex core, and the diameter of the vortex core should be analyzed. Before these analyses, the vortex core should be identified correctly. Vortex classification is a long-studied topic; however, no single definition of a vortex is currently universally accepted. Defining the TLV just based on the streamline (or secondary flow vectors) and the vorticity distribution near the rotor tip may be misleading, because all these identification methods may fail in certain situations [17]. Considering that the TLV is very close to the casing wall where the annulus wall boundary layer exists, the background vorticity magnitude of the shear layer may be comparable to the vorticity magnitude in the core of the TLV. Hence, the center of the core of the TLV is difficult to be distinguished, particularly at the former phases of the TLV because it has a very small size and is almost embedded in the casing wall boundary layer.

There are several popularly used local criteria for identifying the vortex core, such as Q criterion, λ_2 criterion, and Δ criterion; however, not one can be applied without error to all situations. According to the works of Jeong and Hussain [17] and Chakraborty et al. [18], all the aforementioned criteria, which are just based on local flow kinematics (the velocity gradient tensor), have nearly the same capability to distinguish the vortex filaments from the vortex sheets, especially in the case of an intense streamwise vortex. Hence, the particular criteria chosen for the classification of the TLV may have little effect. Studies addressing the application and comparison of these vortex identification criteria in highly turbulent flows also support the preceding statements [19,20]. Here the λ_2 criterion is used for determining the center and the size of the TLV, and the criterion is simplified into the following 2-D form to suit its application for SPIV results:

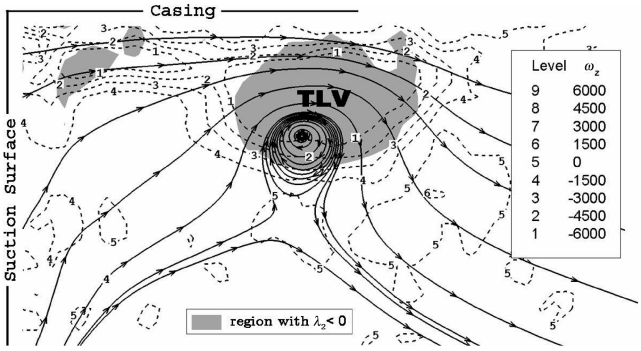

Fig. 5 A representative result is shown for the comparison of the renderings of the TLV by the streamlines (in the reference frame fixed to the rotor blade), the vorticity (indicated by the dotted lines), and the λ_2, respectively.

$$\lambda_2 = (\partial U/\partial x)^2 + (\partial V/\partial y)^2 + 2(\partial U/\partial y)(\partial V/\partial x) \qquad (1)$$

During data processing, the central difference was used to discretize the preceding equation, and the grid of the postprocessed SPIV data was used for calculating directly. A representative result is shown in Fig. 5 for the comparison of the renderings of the TLV by the streamlines, the vorticity, and the λ_2 criterion, respectively. It is evident that the TLV identified by the λ_2 criterion is consistent with the distribution of the high negative vorticity caused by the TLV; however, it separates the TLV from the background high shear layer. Hence, by using the λ_2 criterion, the boundary of the TLV can be detected well.

For the sake of better quantifying the evolution of the TLV, its trajectory, concentration, size, streamwise velocity, and the blockage effect will be discussed in detail next.

1. *Trajectory*

Based on the λ_2 criterion, the TLV is first identified and then the center of the TLV can be determined. As can be seen in Fig. 6, the locations of the center of the TLV core move away gradually from the

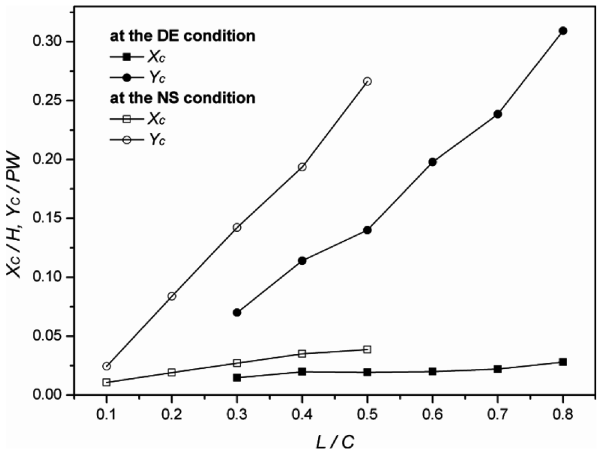

Fig. 6 Variations of the center location of the TLV.

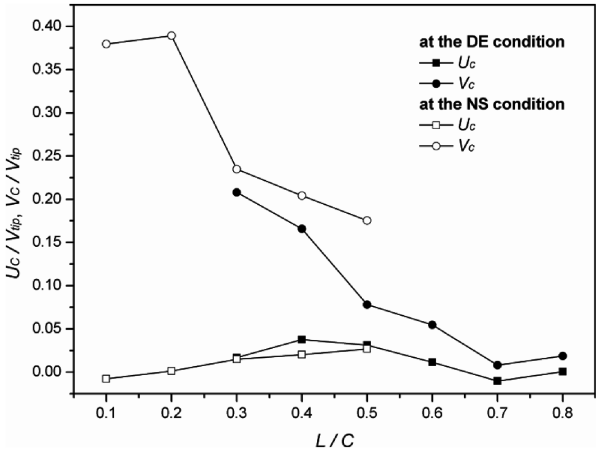

Fig. 7 Variations of the TLV translating velocity relative to the rotor blade.

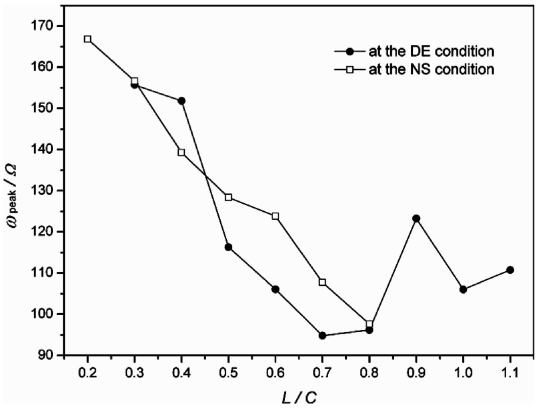

Fig. 8 Variations of the conditional-averaged peak vorticity in the TLV.

blade suction surface (increase of Y_C) and the casing wall (increase of X_C) at both the DE and NS conditions as the vortex progresses downstream. At the DE condition, owing to the TLV becoming highly unstable at $L/C = 0.9$, the region with $\lambda_2 < 0$ splits into several irregular patches. As a result, the λ_2 criterion fails to classify the ensemble-averaged TLV core downstream of this location, indicating that the sample size is inadequate for such highly unsteady flow. For the same reason, at the NS condition, the λ_2 criterion fails downstream $L/C = 0.6$ where the unsteady breakdown of the TLV occurs.

As long as the center of the TLV core is determined, the velocities at the center of the core can be extracted at the center locations. These velocities indicate the moving speed of the TLV away from the rotor blade Y_C and the casing wall X_C, respectively, as shown in Fig. 7. It can be seen that the moving velocities of the TLV are much distinct, particularly in the circumferential direction (direction Y), at both the DE and NS conditions. Thus, analyzing the TLV with the secondary vectors or streamlines at the relative frame fixed to the rotor blade may educe some misleading results. This may be one of the reasons why some researchers did not find well-formed TLV inside the rotor passage or why the trajectories of the TLV they showed were much different.

The center of the TLV moving away from the casing wall may be affected by two effects: the enlargement of the TLV and the entrainment effect of the tip leakage flow. Considering that the upper edges of the TLV core are almost very close to the casing wall, the radial inward moving velocities U_C, as shown in Fig. 7, are mainly caused by the enlargement of the TLV, and thus the increase of X_C may also be mainly caused by the increasing of the vortex's size. As for the circumferential movement of the TLV, the situation is very different. As shown in Fig. 6, the increase of Y_C is steeper at the NS condition than that at the DE condition. This indicates that the TLV moves towards the blade pressure surface faster at the former condition, which can be approved by the discriminations of V_C at different operating conditions shown in Fig. 7, in which V_C is much larger at the NS condition than that at the DE condition. The circumferential movement of the TLV is mainly caused by the entrainment effect of the tip leakage flow, which is determined by the loading of the blade tip. As the compressor operating condition changes from the DE condition to the NS condition, the blade loading moves forward, and the tip leakage flow at the fore-part of the rotor blade intensifies accordingly; as a result, the TLV forms much ahead with higher circumferential translating velocity.

It should be noted that due to the limitation of the spatial resolution of the measurements, the initial points of the TLV are difficult to be exactly determined [16]. Hence, the initial planes at where the TLV are observed may not be its real initial points at both conditions. It can be seen in Fig. 6 that the initial-point displacements of the TLV are not zero at both the DE ($L/C = 0.3$) and NS ($L/C = 0.1$) conditions, indicating that the TLV should arise before these nominal initial planes. Following the evolution trends of Y_C/PW, the TLV may form around $L/C = 0.2$ at the DE condition and a little before $L/C = 0.1$ at the NS condition.

Although the results at the aft part of the TLV trajectory are absent as shown in Fig. 7, their variation tendencies can be seen clearly in Fig. 4. Continuing the trends appearing in Fig. 7, V_C may decrease to a very small value soon after the TLV destabilizes/breaks down at the DE/NS condition, indicating that the low momentum flow in the TLV propagates downstream just carried by the mainstream.

2. *Concentration*

The concentration of a vortex can be expressed by its vorticity magnitude. As mentioned in the previous paper [16], the TLV features unsteady behaviors (wandering, splitting, and breakdown). Moreover, the TLV is also highly asymmetrical for its intense interaction with the flow around it. Taking these factors into account, the simple ensemble-averaged vorticity fields would not be suitable to express the vortex concentration here. To deal with this problem, a conditional-averaged method is employed. By using this method, the peak vorticity in the TLV at each instantaneous realization is extracted individually, and then all the data at the same measurement cross plane are averaged. Evidently, this conditional-averaged peak vorticity, ω_{peak}, can denote the concentration of the unsteady TLV well.

Figure 8 shows the distributions of ω_{peak} in the trajectory of the TLV at different work conditions. At the NS condition, considering that the TLV is so small and close to the casing wall at $L/C = 0.1$, its vorticity value that is affected by the wall shear layer and the laser reflection effect may have low confidence and hence is not shown here. As can be seen in the figure, the peak vorticity decreases almost linearly at the NS condition. Although the TLV breaks down at $L/C = 0.6$–0.8, no abrupt changes of the peak vorticity occur at these locations, which is the main distinction between the results shown in Figs. 8 and 4b. In Fig. 4b, the concentrated vorticity in the TLV expands and falls down suddenly when unsteady vortex breakdown occurs. In fact, as the TLV breaks down, the large concentrated vortex splits into several small distorted vortices. Among these small vortices, some still remain in the streamwise direction, and some others may even change their directions aligning into the cross planes. As a result, the simple ensemble-averaged vorticity magnitude in the TLV falls down abruptly. However, it is reasonable that the vortices remaining in the streamwise direction may still possess high concentration in nearly the same level as their mother vortex. This is why no abrupt changes arise for ω_{peak} as the vortex breakdown occurs.

At the DE condition, the distribution of ω_{peak} is much more complicated than that at the NS condition. ω_{peak} firstly decreases gradually and reaches its minimum value at about $L/C = 0.7$. Then it increases and appears as a local peak at $L/C = 0.9$. After this location, it decreases again. As mentioned in Sec. III.A, the TLV becomes unstable at $L/C = 0.5$–1.0. In fact, the unsteady features of the TLV intensify gradually during this phase. At first, the TLV just

wanders slightly. After which, its wandering magnitude increases. At $L/C = 0.7$, distinct TLV splitting occurs, that is, a large-scale concentrated streamwise vortex splits into several small concentrated streamwise vortices. During this procedure, due to the unsteady interactions between the small streamwise vortices and the main flow and between the small streamwise vortices themselves, the vortex compressing and stretching could occur. As a result, the vorticity magnitudes of the vortices compressed will decrease, and accordingly, the vorticity magnitudes of the vortices stretched will increase. Hence, after $L/C = 0.7$, the increasing of ω_{peak} is reasonable for the stretching of some small vortices. At $L/C = 0.9$, the unsteady behavior of the TLV is the most significant; thus, a peak of ω_{peak} appears. However, due to the viscous diffusion and the vortex interacting effects, the vorticity magnitude in the TLV will decrease finally. After $L/C = 1.0$, the mixing effect dominates the interaction between the flow in the TLV and the mainstream, and the vorticity magnitude in the TLV decreases significantly. Although ω_{peak} is a little larger at $L/C = 1.1$ than that at $L/C = 1.0$, it ought to decrease rapidly downstream at this location.

3. Size

Owing to the approaching of the casing wall, the shape of the TLV is usually elliptical, as shown in Fig. 5. Thus, the diameter of the TLV is defined as the mean of the long and short axes of the $\lambda_2 < 0$ region. The variations of the TLV diameter at the two operating conditions are shown in Fig. 9.

At the NS condition, the TLV always enlarges rapidly as it propagates downstream; however, the rate of its enlargement decreases slowly before the vortex breaks down, and then increases suddenly. The increase of the size of the TLV is caused by the combined effects of vortex engulfment, reinforcing of the tip leakage flow, and the vortex diffusion effect. Considering that the TLV moves quickly away from the blade suction surface, and the tip leakage flow is blocked by the casing wall boundary layer and the up migrating blade boundary layer (i.e., the corner vortex), the TLV will weaken rapidly for the absence of the reinforcement of the tip leakage flow in the flow condition with strong adverse pressure gradient. As a result, the vortex engulfment will decrease soon, and the rate of vortex enlargement should decrease.

As for the DE condition, the enlargement rate at the fore part of the TLV is a little less than that at the NS condition, indicating also that the TLV and the tip leakage flow are weaker at the DE condition. As the TLV forms, the enlargement rate of the TLV stays almost in a constant value before the vortex becomes highly unsteady at $L/C = 0.7$. After this location, the increase of the TLV diameter becomes faster than before. As mentioned in Sec. III.B.1, the circumferential translating velocity of the TLV is much slower at the DE condition, and as shown in Fig. 4a, there are almost no low-momentum flows stacking at the suction tip corner. Therefore, the tip leakage flow reinforcing effect can persist for a much longer time. Moreover, the adverse pressure gradient is also much gentler at the DE condition. As a result, the enlargement of the TLV can stay at a nearly constant rate when it is stable enough. However, as the TLV becomes unstable, the vortex wandering and splitting can intensify the diffusion effect. As a result, the enlargement rate of the TLV may even increase.

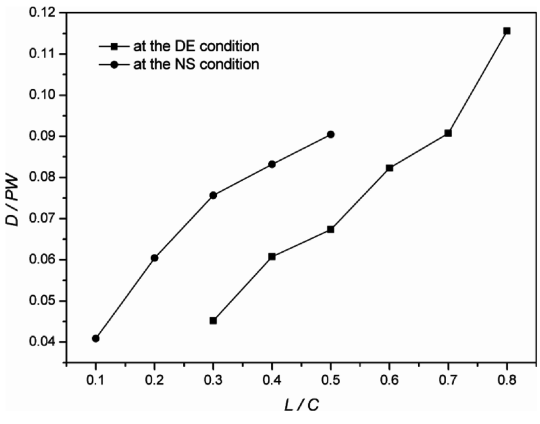

Fig. 9 Variations of the TLV diameter.

It should be noted that the vortex diameters extracted based on the ensemble-averaged results may mislead when the vortex wanders, because their values should be larger than the real ones [21]. Hence, in Fig. 9, the values of the TLV diameter at the locations after the TLV becomes unstable are a little larger than their real values. However, these data can denote the area affected by the TLV, which is useful for the analyses of the flow loss and blockage inside the rotor passage.

4. Streamwise Velocity

Both the variations of W_{min} (the minimum streamwise velocity in the TLV core) and W_C (the streamwise velocity at the center of the TLV core) are shown in Fig. 10a. These two parameters are all normalized by W_{ext}, which is the local mean streamwise velocity at the outer edge of the TLV core. Based on this kind of normalization, the flow decay characteristics in the core of the TLV can be shown well. Moreover, it should be noted that the results extracted from the SS and PS planes are discontinuous, which is caused by the intersection of the two groups of planes, as mentioned in Sec. II.C.

As can be seen in Fig. 10a, it is evident that the TLV is a wakelike streamwise vortex at both the two operating conditions. The results also indicate that the TLV is highly skewed, because W_{min} is not located at the center of the vortex at most times. At the initial stage of the TLV, W_{min} usually appears at the upper-right side of the TLV,

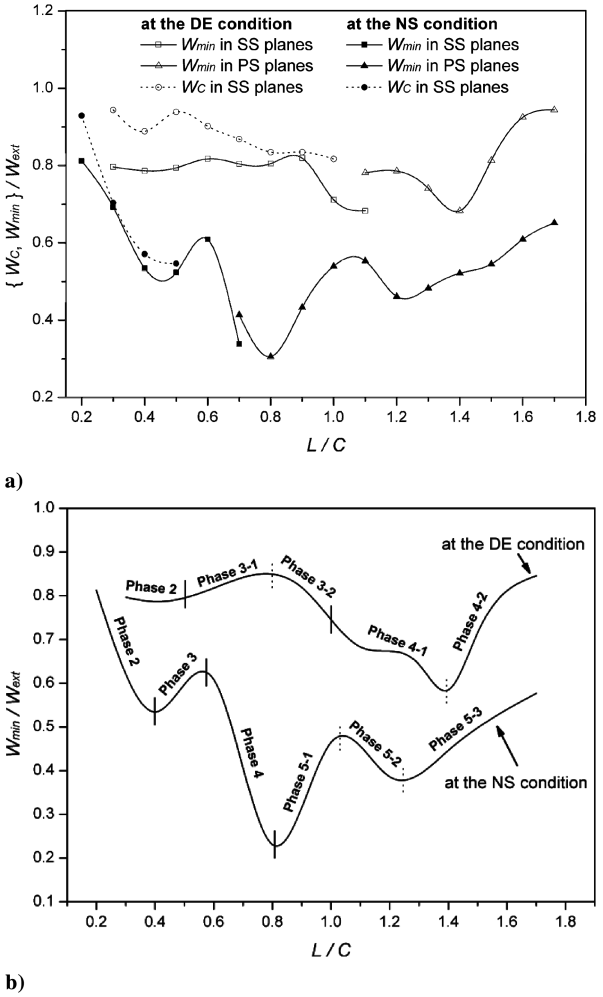

Fig. 10 Variations of the minimum streamwise velocity in the TLV core and the streamwise velocity at the center of the TLV core. a) Experimental results; b) general evolution trends of $W_{\text{min}}/W_{\text{ext}}$.

where the interaction between the tip leakage flow and the annulus wall boundary layer is most intense. It is well known that the streamwise velocities of both the tip leakage flow and the annulus wall boundary layer are very low. Hence, W velocity should also be very low at their interacting region. However, as the tip leakage flow turns inward and rolls up into the TLV, the low-momentum flow is energized by the mainstream, and its streamwise velocity increases. As a result, W_C is usually a little larger than $W_{\min}$ at the fore part of the TLV trajectory. As the TLV propagates downstream, the interaction between the tip leakage flow and the casing wall boundary layer weakens, and owing to the viscous diffusion effect and the kinematic features of the quasi-cylindrical vortex, the location of $W_{\min}$ migrates close to the center of the vortex core appearing as there is a decrease of the disparity between $W_{\min}$ and W_C.

It can be seen in Fig. 10a that the disparity between $W_{\min}$ and W_C decreases much more quickly at the NS condition than at the DE condition, indicating again that the intense tip leakage flow affects the TLV just at the fore part of the blade tip clearance at the NS condition. It can also be seen that after the locations at where $W_{\min}$ and W_C overlap ($L/C = 0.9/0.3$ at the DE/NS condition), they separate again. This may result from the enhancement of vortex destabilization. Thus, the asymmetry of the TLV is mainly caused by its unsteady behaviors at the aft part of its trajectory.

For easy analysis, the general evolution trends of the normalized $W_{\min}$ are replotted in Fig. 10b. Different evolution phases of the TLV indicated in Sec. III.A are also labeled in the figure, and some phases are divided into several subphases based on the change of the evolution tendencies of the normalized $W_{\min}$. Considering that the data extracted from the PS planes can also show the right evolution trends of the TLV, we just simply transfer the curves of the PS planes in Fig. 10a down to make the curves link together in Fig. 10b.

At the DE condition, the normalized $W_{\min}$ decreases slightly first in phase 2. This is reasonable for the streamwise velocity variation of an expanded quasi-cylindrical vortex core, as analyzed by M. G. Hall [22]. However, as the TLV propagates downstream, it soon becomes unstable. As indicated in Sec. III.B.2, in phase 3, the unsteadiness of the TLV intensifies gradually. The vortex first wanders slightly, and then its wandering's magnitude increases. Finally, the TLV splitting occurs. It is evident that due to vortex wandering, $W_{\min}$ should be a little larger than its real value in the ensemble-averaged results; meanwhile, the mixing effect will increase. As a result, the decrease of $W_{\min}$ is retarded, and the normalized $W_{\min}$ even increases slightly in phase 3–1. As the vortex splitting occurs, the low-momentum flow in the TLV expands rapidly, as can be seen in Fig. 4a. During this procedure, owing to the potential effect of the low-momentum flow, a local high-speed region appears around the TLV (see also Fig. 4a), resulting in the retardation of the decrease of W_{ext}. Hence, the normalized $W_{\min}$ decreases rapidly in phase 3–2. It can be seen in Fig. 4a that the potential effect of the TLV is prominent even far downstream, and thereby the normalized $W_{\min}$ decreases continuously in phase 4–1. Because of the increase of the turbulence mixing effect in phase 4, the normalized $W_{\min}$ increases finally in phase 4–2.

There are five distinct phases in the evolution procedure of the TLV at the NS condition. As a whole, the normalized $W_{\min}$ is lower at the NS condition than that at the DE condition. In phases 2 and 3, the normalized $W_{\min}$ decreases and increases with the same mechanisms as that indicated at the DE condition in phases 2 and 3–1; however, they are much steeper because the rotating of the TLV is more intense, and the nonlinear increase of the unsteadiness of the TLV is much more remarkable at the NS condition than that at the DE condition. In phase 4, the normalized $W_{\min}$ decreases rapidly. As indicated in Sec. III.A, the unsteady vortex breakdown occurs in this phase, that is, unsteady flow stagnation/reverse appears in the core of the TLV. Hence, due to the combined effects of the rapid decrease of $W_{\min}$ and the potential effect of the TLV, the normalized $W_{\min}$ decreases rapidly. Downstream of the vortex breakdown region, $W_{\min}$ recovers and increases significantly; as a result, the normalized $W_{\min}$ rises in phase 5–1. However, as $W_{\min}$ increases to a reasonable value, it decreases again [16]. Then owing to the potential effect of the TLV (see Fig. 4b), the normalized $W_{\min}$ decreases again in phase 5–2. At last, in phase 5–3, the normalized $W_{\min}$ increases and tends to unity due to the turbulence mixing effect, which is the same as that in phase 4–2 at the DE condition.

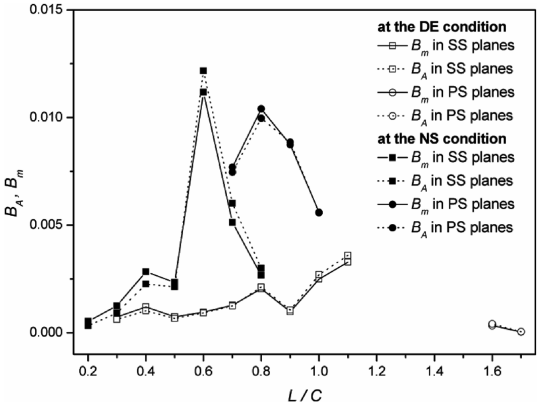

Fig. 11 Variations of the blockage coefficient caused by the TLV.

5. Blockage Effect

A frequently used blockage coefficient is defined as

$$B_A = A_b/A_p = \int_{A_e} (1 - W/W_{\text{ext}})\, \mathrm{d}A/A_p \tag{2}$$

This parameter denotes how large an area is blocked by the low momentum flow, which is similar to the definition of the displacement thickness of the boundary layer. Based on this definition, the variations of the area-based blockage coefficient of the TLV are plotted in Fig. 11. However, it should be noted that W_{ext} is just the local mean streamwise velocity at the outer edge of the TLV core. As we know, the streamwise velocity varies significantly inside the blade passage, particularly at the NS condition. As a result, B_A may sometimes over- or underestimate the actual blockage effect.

Considering that the blockage affects the mass flow rate directly, we define a mass-flow-based blockage coefficient as

$$B_m = m_b/m_t = \rho \int_{A_e} (W_{\text{ext}} - W)\, \mathrm{d}A/m_t \tag{3}$$

It denotes the normalized mass flow rate blocked by the TLV. This is a useful parameter for the concept of flow control. The variations of B_m are also shown in Fig. 11. It is evident that B_m and B_A are very close, especially at the DE condition.

It is clear that the blockage caused by the TLV is much higher at the NS condition than that at the DE condition. As the TLV becomes unstable/breaks down, its blockage increases significantly. The maximum blockage mass flow rate is about 1.12% of the total mass flow rate at the NS condition; however, it is about 0.33% at the DE condition. Comparing Figs. 10 and 11, it can be found that as the normalized $W_{\min}$ decreases the blockage may not increase. Hence, the normalized $W_{\min}$ cannot denote the blockage effect caused by the TLV.

C. Typical Unsteady Features

Based on the preceding analyses, it can be concluded that the unsteady behaviors of the TLV have profound effects to its mean flow characteristics. As mentioned before, the TLV has several distinct unsteady behaviors, including vortex wandering, splitting, and breakdown. Therefore, it is necessary to explore the unsteady features of the TLV for obtaining a thorough knowledge of it. To analyze the unsteady behaviors of a concentrated vortex, appropriate conditional-averaged methods are often employed. Van der Wall and Richard introduced a method for analyzing SPIV data acquired from a rotor test to study the properties of the wing tip vortex [20]. By using the vortex center positions identified by an improved λ_2 criterion, they compared the vortex properties obtained by using conditional averaging, in which all vortex centers were shifted to

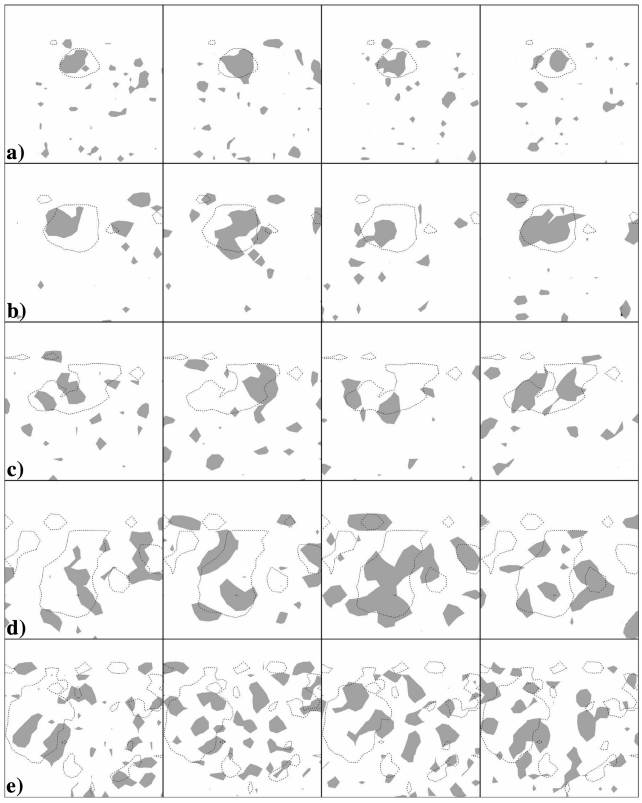

Fig. 12 Representative instantaneous realizations of the TLV at $L/C=$ a) 0.3, b) 0.5, c) 0.7, d) 0.9, e) 1.1 at the DE condition. (Dotted lines indicate vortices in the ensemble-averaged results, and gray regions indicate vortices in the instantaneous snapshots. Vortices are identified by the λ_2 criterion.)

coincide with each other, and simple averaging (ensemble averaging). They concluded that the conditional-averaging method was superior to the simple averaging method and that it was important to apply this methodology when analyzing the characteristics of a concentrated vortex. Oweis and Ceccio investigated the interaction between the tip leakage vortex and the blade wake on a ducted propulsor using PIV [23]. To analyze their PIV data, they used a vortex reconstruction method in which ideal Gaussian vortices were fitted to the multiple vortices in the flowfield identified by local peaks in the vorticity field. As a result, they could analyze in detail the properties of different vortices and the vortex-induced pressure variations with conditional averaging. Although the identification of the vortex locations using local peaks in the vorticity field is not precise, it was acceptable in their case because the flowfield they investigated had no regions of high shear layer. Besides the conditional-averaged methods mentioned earlier, there are also some other methods, such as proper orthogonal decomposition (POD) and small-eddy decomposition, that can be applied to flows of this type [19]. Despite this, the selection of a conditional-averaging method for the present case is not straightforward. There are two specific difficulties. First, the TLV is highly skewed and so its center is difficult to be accurately defined. Second, the TLV splits into several small vortices when it becomes unstable, and their states often change completely in different instances. It is possible that wavelets- or POD-based methods are suitable for further analysis of the unsteady behavior of the TLV, because they can extract structures (with high energy) from highly turbulent flows. This has not, however, been investigated in the current work. Herein, we will just show some results for direct observation of the unsteady features of the TLV.

Some typical instantaneous results are shown in Fig. 12. It can be seen clearly that the TLV is indeed a flow structure with intense unsteady behaviors. Although the TLV forms near $L/C = 0.3$ at the DE condition, it varies in shape and in size, and wanders slightly at different instants. At $L/C = 0.5$, the wandering magnitude of the

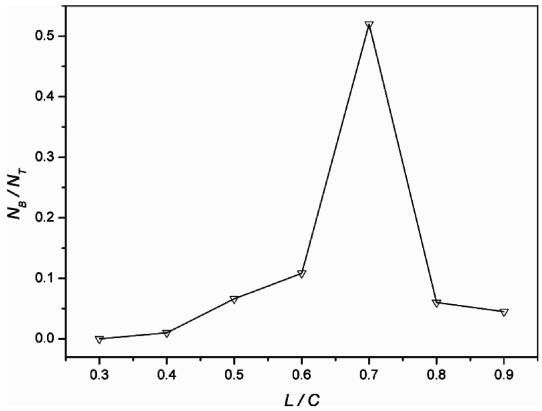

Fig. 13 Probabilities for the occurrence of the TLV breakdown in different measurement planes at the NS condition.

TLV increases remarkably, and it seems that the vortex splitting incepts. At $L/C = 0.7$, distinct vortex splitting can be seen clearly. Comparing the results at $L/C = 0.7$ and $L/C = 0.9$, it can be found that due to continuous vortex splitting, the number of vortex patches increases as the TLV propagates downstream; however, their sizes do not decrease, indicating that most of the vortex patches still possess the features of a concentrated streamwise vortex. Finally, at $L/C = 1.1$, where the turbulence mixing effect dominates the flow, it is difficult to distinguish the TLV from the instantaneous snapshots, because the small vortex patches distribute all over the blade tip region, and their sizes decrease distinctly. It should be noted that the core of the TLV skews prominently in the ensemble-averaged flowfields after $L/C = 0.7$, indicating that the data sets are inadequate for the ensemble averaging analyses of such highly unsteady flow. Another thing that should be noted is that the core of the TLV in the instantaneous flowfields is always smaller than that in the ensemble-averaged results. In addition, as the vortex wandering magnitude increases, the disparity between the sizes of the instantaneous TLV and ensemble-averaged TLV increases.

The existence of the TLV breakdown was confirmed by catching the vision of the flow stagnation or flow reverse from the experimental results shown in the authors' previous paper [16]. In that paper, the TLV breakdown with unsteady feature was noticed; however, no results were provided to quantify its unsteady behavior. According to the statistics of all the instantaneous realizations, the variations of the occurrence probability of the TLV breakdown are obtained and are shown in Fig. 13. It can be seen that the TLV breakdown happens in a very wide range from $L/C = 0.4$ to $L/C = 0.9$, where flow stagnation or flow reverse exists. In contrast, the occurrence probabilities of the vortex breakdown are very low at most locations, except at $L/C = 0.7$, where more than half of the instantaneous snapshots have flow reverse or flow stagnation. Although the flow stagnation and flow reverse arise at $L/C = 0.7$ frequently, the minimum streamwise velocity is about 11 m/s at this plane in the TLV region in the ensemble-averaged flowfield, which is mainly caused by the moment-to-moment variations of flow reverse and stagnation.

IV. Conclusions

The flowfields in the tip region of the rotor passage were investigated from a large-scale low-speed axial compressor test at both the design and near-stall conditions by using SPIV. In the present study, the measurement data related to the TLV were analyzed. To better quantify the characteristics of the TLV, its trajectory, concentration, size, streamwise velocity, and the blockage effect were extracted from both the ensemble- and conditional-averaged results. Some main results about the tested compressor are summarized as follows:

1) The TLV undergoes four distinct evolution phases at the DE condition: formation, evolution and expansion, destabilization, and turbulence mixing. However, there are five evolution phases of the

TLV at the NS condition: formation, evolution and expansion, destabilization, unsteady breakdown, and turbulence mixing.

2) Although the TLV breaks down at the NS condition, the conditional-averaged peak vorticity, ω_{peak}, in the core of the TLV appears to have no abrupt changes due to the existence of the small concentrated streamwise vortices; however, a sudden decrease of the vorticity magnitude in the ensemble-averaged result happens. At the DE condition, ω_{peak} reaches a minimum value and then increases during the destabilization phase of the TLV because of the stretching of the split small streamwise vortices.

3) The TLV enlarges rapidly as it propagates downstream at the NS condition; however, its enlargement rate decreases slowly before the vortex breaks down, and then increases suddenly. At the DE condition, the enlargement rate of the TLV stays almost in a constant value in the fore-part of the vortex trajectory, and then due to the increase of the vortex wandering magnitude, it even increases.

4) The TLV is highly skewed, because W_{min} is not located at the center of the vortex core at most times at both the DE and NS conditions, especially in its formation phase. However, as the TLV progresses downstream, the location of W_{min} migrates gradually to the center of the vortex core.

5) Because of multiple factors, including the kinematic features of the quasi-cylindrical vortex, vortex wandering, the potential effect of low momentum flow, and the turbulence mixing effect, the normalized W_{min} varies up and down at different evolution phases of the TLV.

6) A mass-flow-based blockage coefficient is defined in the paper, and the results show that the maximum blockage mass flow rate is about 1.12% of the total mass flow rate at the NS condition; however, it is about 0.33% at the DE condition.

7) The TLV in the tested compressor possesses several typical unsteady behaviors, including vortex wandering, splitting, and breakdown, which have profound effects to the mean flow characteristics of the TLV. At the DE condition, the most significant unsteady behaviors of the TLV are vortex wandering and splitting. As for the NS condition, unsteady vortex breakdown appears.

Acknowledgments

The authors would like to acknowledge the support of National Science Foundation of China, Grant No. 50006001 and No. 50476001, and the support of National Foundation Research Project, Grant No. 1999022305.

References

[1] Wisler, D. C., "Loss Reduction in Axial Flow Compressors Through Low-Speed Model Testing," *Journal of Turbomachinery*, Vol. 107, April 1985, pp. 354–363.

[2] Adamczyk, J. J., Celestina, M. L., and Greitzer, E. M., "The Role of Tip Clearance in High-Speed Fan Stall," *Journal of Turbomachinery*, Vol. 115, Jan. 1993, pp. 28–38.

[3] Inoue, M., Kuroumaru, M., Yoshida, S., Minami, T., Yamada, K., and Furukawa, M., "Effect of Tip Clearance on Stall Evolution Process in a Low-speed Axial Compressor Stage," ASME Paper 2004-GT-53354, 2004.

[4] Peacock, R. E., "A Review of Turbomachinery Tip Gap Effects, Part 2: Rotating Machinery," *International Journal of Heat and Fluid Flow*, Vol. 4, No. 1, 1983, pp. 3–16.

[5] Inoue, M., Kuroumaru, M., and Fukuhara, M., "Behavior of Tip Leakage Flow Behind an Axial Compressor Rotor," *Journal of Engineering for Gas Turbines and Power*, Vol. 108, No. 1, 1986, pp. 7–14.

[6] Lakshminarayana, B., and Murthy, K. N. S., "Laser Doppler Velocimeter Measurement of Annulus Wall Boundary Layer Development in a Compressor Rotor," *Journal of Turbomachinery*, Vol. 110, No. 3, 1988, pp. 377–385.

[7] Inoue, M., and Kuroumaru, M., "Structure of Tip Clearance Flow in an Isolated Axial Compressor Rotor," *Journal of Turbomachinery*, Vol. 111, No. 3, 1989, pp. 250–256.

[8] Storer, J. A., and Cumpsty, N. A., "Tip Leakage Flow in Axial Compressors," *Journal of Turbomachinery*, Vol. 113, No. 2, 1991, pp. 252–259.

[9] Moyle, I. N., Walker, G. J., and Shreeve, R. P., "Stator Averaged, Rotor Blade-to-Blade Near Wall Flow in a Multistage Axial Compressor With Tip Clearance Variation," *Journal of Turbomachinery*, Vol. 114, No. 3, 1992, pp. 668–674.

[10] Kang, S., and Hirsch, C. H., "Experimental Study on the Three-Dimensional Flow Within a Compressor Cascade with Tip Clearance: Part 1—Velocity and Pressure Fields," *Journal of Turbomachinery*, Vol. 115, No. 3, 1993, pp. 435–443.

[11] Lakshminarayana, B., Zaccaria, M., and Marathe, B., "The Structure of Tip Clearance Flow in Axial Flow Compressors," *Journal of Turbomachinery*, Vol. 117, No. 3, 1995, pp. 336–347.

[12] Inoue, M., Kuroumaru, M., Saiki, K., and Yamada, K., "The Role of Tip Leakage Vortex Breakdown in Compressor Rotor Aerodynamics," *Journal of Turbomachinery*, Vol. 121, No. 3, 1999, pp. 469–480.

[13] Liu, B. J., Wang, H. W., Liu, H. X., Yu, H. J., Jiang, H. K., and Chen, M. Z., "Experimental Investigation of Unsteady Flow Field in the Tip Region of an Axial Compressor Rotor Passage at Near Stall Condition with Stereoscopic Particle Image Velocimetry," *Journal of Turbomachinery*, Vol. 126, No. 3, 2004, pp. 360–374.

[14] Wernet, M. P., Zante, D. V., Strazisar, T. J., John, W. T., and Prahst, P. S., "3-D Digital PIV Measurements of the Tip Clearance Flow in an Axial Compressor," ASME Paper 2002-GT-30643, 2002.

[15] Uzol, O., Chow, Y. C., Soranna, F., and Katz, J., "3D Structure of Rotor Wake at Mid-Span and Tip Regions," AIAA Paper 2004-2552, 2004.

[16] Liu, B. J., Yu, X. J., Yuan, H. J., Liu, H. X., Jiang, H. K., and Xu, Y. T., "Application of SPIV in Turbomachinery," *Experiments in Fluids*, Vol. 40, April 2006, pp. 621–642.

[17] Jeong, J., and Hussain, F., "On the Identification of a Vortex," *Journal of Fluid Mechanics*, Vol. 285, Feb. 1995, pp. 69–94.

[18] Chakraborty, P., Balachandar, S., and Adrian, A. J., "On the Relationships Between Local Vortex Identification Schemes," *Journal of Fluid Mechanics*, Vol. 535, July 2005, pp. 189–214.

[19] Adrian, R. J., Christensen, K. T., and Liu, Z.-C., "Analysis and Interpretation of Instantaneous Turbulent Velocity Fields," *Experiments in Fluids*, Vol. 29, Sept. 2000, pp. 275–290.

[20] van der Wall, B. G., and Richard, H., "Analysis Methodology for 3C-PIV Data of Rotary Wing Vortices," *Experiments in Fluids*, Vol. 40, May 2006, pp. 798–812.

[21] Straka, W. A., and Farrell, K. J., "The Effect of Spatial Wandering on Experimental Laser Velocimeter Measurements of the End-Wall Vortices in an Axial-Flow Pump," *Experiments in Fluids*, Vol. 13, Jan. 1992, pp. 163–170.

[22] Hall, M. G., "The Structure of Concentrated Vortex Cores," *Progress in Aeronautical Sciences*, Vol. 7, No. 2, 1966, pp. 53–110.

[23] Oweis, G. F., and Ceccio, S. L., "Instantaneous and Time-Averaged Flow Fields of Multiple Vortices in the Tip Region of a Ducted Propulsor," *Experiments in Fluids*, Vol. 38, May 2005, pp. 615–636.

F. Coton
Associate Editor